A major purpose of the Technical Information Center is to provide the broadest dissemination possible of information contained in DOE's Research and Development Reports to business, industry, the academic community, and federal, state and local governments.

Although a small portion of this report is not reproducible, it is being made available to expedite the availability of information on the research discussed herein.

LA-UR -85-3026

CONF-850[illegible]--8

Los Alamos National Laboratory is operated by the University of California for the United States Department of Energy under contract W-7405-ENG-36.

LA-UR--85-3026

DE85 017533

TITLE: HIGH STRAIN RATE DEFORMATION IN FCC METALS AND ALLOYS

MASTER

AUTHOR(S): P. S. Follansbee

SUBMITTED TO: Explomet '85', International Conference on Metallurgical Applications of Shock-Wave and High-Strain-Rate Phenomena, Portland, OR, July 28-August 1, 1985.

DISCLAIMER

Los Alamos Los Alamos National Laboratory
Los Alamos, New Mexico 87545

HIGH STRAIN RATE DEFORMATION IN FCC METALS AND ALLOYS

P. S. Follansbee
Los Alamos National Laboratory
Los Alamos, New Mexico, USA, 87545

The effect of strain rate, and particularly of high strain rates, on deformation mechanisms in materials is of fundamental interest to those who model and analyze dynamic loading. In many materials the strain rate sensitivity is known to increase dramatically when the strain rate is raised above ~10^3 s^{-1}. This increase has been interpreted previously as a transmition in deformation mechanism from thermal activation control at low strain rate to dislocation drag control at high strain rate. In copper, copper-aluminum alloys and stainless steel, recent measurements have shown that the increased rate sensitivity found at high strain rates is not due to a transition in deformation mechanism but rather can be explained with standard thermal activation theory. These findings and their implications regarding the formulation of constitutive behavior will are presented.

I. INTRODUCTION

Although the high strain rate deformation behavior of most common metals has been studied using one of a variety of experimental techniques [1], studies of FCC metals using techniques based on the Hopkinson bar have

dominated the literature. Some of these investigations are listed in Table 1. This tabulation is not meant to be all inclusive, b.: rather to list those investigations where the constant strain, strain rate sensitivity, which is defined as

$$M_\varepsilon = \frac{\partial \sigma}{\partial \log \dot{\varepsilon}}\Big]_\varepsilon , \tag{1}$$

could be evaluated over a wide range of strain rates. The high strain rate data in most of these investigations have been measured in compression using the split Hopkinson pressure bar.

In many of the references listed in Table 1, the constant strain, strain rate sensitivity is found to increase when the strain rate is raised above roughly 10^3 s^{-1}. When the maximum strain rate investigated is limited to 10^3 s^{-1}, such an increase is usually not seen [3,5,10]. This increase or transition in rate sensitivity has been the topic of much discussion. Although in polycrystalline copper, most previous investigators have noted such a transition when strain rates of the order 10^4 are achieved, Lindholm [11] have did not measure any increase in rate sensitivity at strain rates as high as $6x10^4$ s^{-1}. This has led to questions concerning the validity of experimental techniques at these high strain rates. Whether or not there exists an increase in the rate sensitivity at high strain rates is an important question. Many impact phenomena lead to deformation at strain rates exceeding 10^3 s^{-1}; the ability to model these processes computationally requires the knowledge and understanding of the material constitutive behavior at high strain rates.

Explanations for the increased rate sensitivity have been proposed which are based on a transition in rate controlling deformation mechanism from thermal activation at low strain rates to some form of dislocation drag, due to the interactions with phonons at room temperature [22], at strain rates exceeding 10^3 s^{-1}. The predominance of dislocation drag controlled deformation has been used to explain the experimentally observed relationship between flow stress σ (at constant strain) and strain rate $\dot{\varepsilon}$,

$$\sigma = \sigma_b + \beta\dot{\varepsilon} , \tag{2}$$

where the back stress σ_b and the constant β are both functions of strain. There has been wide usage of "viscous" or "linear" laws such as Eq. 2 to describe constitutive behavior at high strain rates.

The purpose of this paper is to describe the dynamic deformation behavior of a few FCC metals. First, we will briefly review the split Hopkinson pressure bar experimental techniques and specifically address the question of test validity. We conclude that valid test results are obtainable at strain rates approaching and even exceeding 10^4 s^{-1} if certain precautions are taken. Some experimental results obtained in copper, copper-aluminum alloys, and five austenitic stainless steels will be presented in Section 3. In Section 4 the origin of the increased rate sensitivity at high strain rates is discussed. In order to investigate the role of dislocation drag mechanisms, the current understanding of dislocation glide kinetics is reviewed. Dynamic flow stress measurements are compared with measurements of the mechanical threshold stress, which is used as an internal state variable, and it is concluded that dislocation drag mechanisms do not contribute to the rate sensitivity in the FCC metals investigated at strain rates less than 10^4 s^{-1}. An alternate explanation for the increased rate sensitivity, based on structure evolution, is proposed. The influence of these findings on the appropriate formulation of a constitutive law is described in Section 5.

II. DYNAMIC TESTING WITH THE HOPKINSON BAR

Experimental techniques based on the Hopkinson pressure bar are well-developed; for discussion of these techniques, the reader is referred to reviews by Lindholm [3,23] and Follansbee [24]. In the latter reference the topic of test validity is discussed and it is shown that, in the compression test with the split Hopkinson pressure bar (SHPB), factors that influence test validity include frictional constraint, radial and axial inertial constraint, and elastic wave dispersion. In addition, the correct specification of timing between the three strain gage signals becomes increasingly critical at high strain rates. The problem of friction accompanies compression testing at all strain rates, and the problem is not influenced greatly by the actual strain rate. A great deal is known about lubrication techniques and specimen aspect ratios (l/d where l is the specimen length and d is the diameter) that minimize errors due to frictional constraint. Unfortunately, the optimum aspect ratio suggested for a quasi-static compression test ($1.5 \leq l/d \leq 2$) should not be used in the SHPB test because of inertial constraint considerations. In an early

analysis of the errors due to radial and axial constraint in a rapidly deforming solid cylinder, Davies and Hunter [25] concluded that these errors would be minimized if the aspect ratio of a specimen deforming at constant strain rate were chosen such that

$$\frac{l}{d} = \left(\frac{3\nu_s}{4}\right)^{1/2} , \tag{3}$$

where ν_s is the Poisson ratio. Note that for $\nu_s = 1/3$, Eq. 3 yields $l/d = 0.5$.

Bertholf and Karnes [26] performed a full two-dimensional, finite difference, elasto-plastic analysis of the SHPB test and found results consistent with Eq. 3. Furthermore, these authors investigated test validity up to a strain of ~ 4% and concluded that if the loading wave were a trapezoidal wave of risetime T_r rather than a square wave, then test results were valid providing that

$$D\,\dot{\varepsilon} < 5\times10^{3}\ \text{cm-s}^{-1} \tag{4}$$

and

$$\frac{T_r}{D} > 16\ \mu\text{s-cm}^{-1} , \tag{5}$$

where D is the diameter of the pressure bar. Dispersion in the elastic pressure bar will naturally decrease the slope in the leading edge of the loading wave. Techniques to further increase the risetime of this wave have been described by Frantz et al [27]; it is not difficult to approximate the trapezoidal wave condition imposed by Bertholf and Karnes. The criteria of Eqs. 4 and 5 suggests that for tests with 5 mm diameter pressure bars, test results at strain rates as high as $10^4\ s^{-1}$ can be performed if the l/d ratio of the specimen is chosen to match Eq. 3 and if normal lubrication techniques are employed. Inspection of the actual results in [26] suggests that the criteria of Eq. 4 may be slightly overconservative. Indeed, if test validity had been evaluated at a higher strain than 4%, higher strain rates would have been allowed.

Another problem with experiments in the Hopkinson bar arises in the interpretation of the strain gage signals. Recall that one of the advantages of test techniques based on the Hopkinson bar is that the stress and strain in the deforming sample are simply related to strain gage measurements made on the elastic pressure bars. For the split Hopkinson pressure bar shown schematically in Fig. 1, the initial compressive wave

$E_I(t)$ and reflected tensile wave $E_R(t)$ measured on the incident bar and the transmitted compressive wave $E_T(t)$ measured on the transmitter bar can be combined to yield the stress within the specimen according to

$$\sigma(t) = \frac{E}{2}\frac{A}{a_o}\left[E_I(t)+E_R(t)+E_T(t)\right] \tag{6}$$

and the strain within the sample according to

$$\varepsilon(t) = \int \frac{C_o}{l_o}\left[E_I(t)-E_R(t)-E_T(t)\right] dt \ , \tag{7}$$

where E is Young's modulus, C_o is the longitudinal wave velocity, a_o and l_o are the initial cross sectional area and length of the specimen, and A is the cross sectional area of the pressure bar. Typically it is assumed that the stress on both faces of the specimen (and throughout the specimen) is constant at any time, which implies that

$$E_T(t) = E_I(t)+E_R(t) \tag{8}$$

and simplifies Eqs. 6 and 7 to read

$$\sigma(t) = E\frac{A}{a_o}E_T(t) \ , \tag{9}$$

and

$$\varepsilon(t) = \int \frac{-2C_o}{l_o}E_R(t)\,dt \ . \tag{10}$$

When Eq. 8 applies, measurement of the reflected and transmitted strain gage signals determines the stress strain behavior in the deforming specimen. The operational problem with this lies in establishing the precise timing between these waves. Usually, it is assumed that placing strain gages equidistant from the sample assures that the strain gage signals correlate in real time. However, the precise timing between the three waves will be influenced by imperfect interfaces, the presence of lubricants and the transit time through the specimen. Elastic wave dispersion will combine with the sources of error listed above to complicate the selection of "zero" time with which to start the integration in Eq. 10. The combined effect of these errors is small (e.g., an uncertainty of $\mp$ 10μs in the timing relationship), but can have a large influence on the predicted stress strain curve as the strain rate is increased, or as the total test time is decreased.

To minimize these errors we have added several calibration routines to

our SHPB test procedure. First of all, we establish actual timing between E_I and E_R by firing the striker bar at the incident bar which is separated from the transmitter bar. Secondly, we establish actual timing between E_I and E_T by firing the striker bar at the incident bar which is in direct contact with the transmitter bar (i.e., no specimen). During this calibration run we also verify gage factors for both strain gages by accurately measuring the striker bar velocity and using the momentum balance expression given by Lindholm [3]. In addition to these calibration procedures, we have chosen to use Eqs. 6 and 7 rather than Eqs. 9 and 10 to compute stress and strain within the deforming specimen. The advantage of this is that it reduces the uncertainty in the timing since the timing between E_I and E_R has been accurately established. Secondly, it allows the use of E_I, which is the most sharply rising wave, to establish "zero" time. The disadvantage of this procedure is that it introduces larger Pochhammer-Chree oscillations into the stress strain curve which do not truly represent behavior within the specimen. The extent of this problem can be minimized by performing a dispersion correction on all three waves to "move" them to the specimen interfaces [28].

An example of a stress strain curve measured in Nitronic 40 at a strain rate of ~ 6000 s^{-1} is shown in Fig. 2. The solid curve shown in Fig. 2 is the result derived using Eqs. 6 and 7 while the dashed curve is the result derived using Eqs. 9 and 10. The agreement in this case is good which gives confidence in the test procedure and result. At higher strain rates, the two curves sometimes do not agree as well; in these cases we choose the 3-wave (Eqs. 6 and 7) rather than the 2-wave analysis.

With the procedures outlined above, we have a high degree of confidence in our SHPB test results at strain rates as high as ~1.5×10^4 s^{-1}. In the next section some experimental results on a variety of FCC metals will be presented.

III. EXPERIMENTAL RESULTS IN SOME FCC METALS

The stress strain behavior of oxygen-free electronic copper and several copper aluminum alloys and austenitic stainless steels in compression has been determined over a wide range of strain rates. Data at strain rates from 10^3 s^{-1} to ~1.5×10^4 s^{-1} were measured using the SHPB test procedure described in the previous section. Strain rates from 10^{-4} s^{-1} to 10^{-1} s^{-1}

were achieved in a standard screw-driven mechanical testing machine while data at strain rates from 10^{-1} s^{-1} to 10^{2} s^{-1} were measured using a servo-hydraulic testing machine with an optical extensometer. Extent of deformation was generally limited to less than a true strain of 30%. All materials were investigated in the recrystallized condition with average grain dimension of order 30 μm to 50 μm. The compositions of the stainless steels are shown in Table 2.

When testing over the wide range of strain rates indicated above there is a transition from isothermal test conditions to adiabatic test conditions. In the latter case, the temperature rise in the specimen due to conversion of plastic work into heat is given by

$$\Delta T = \frac{\psi}{\rho C_p} \int \sigma(\varepsilon)\, d\varepsilon \ , \qquad (11)$$

where ρ is the density, C_p is the heat capacity and ψ is the fraction of work converted into heat ($\psi \approx 1$). Table 3 lists approximate values of ρC_p and $\int \sigma(\varepsilon) d\varepsilon$ for copper and Nitronic 40 deformed to a strain of 0.20 at strain rates of 6×10^{3} s^{-1} and 5×10^{3} s^{-1} respectively. (See Figs. 3 and 4). Included in this table are the temperature increases estimated from Eq. 11 and the corresponding decreases in flow stress (estimated from Eqs. 14 and 15 and data presented in the following section). It is evident that the temperature rise and flow stress increment are relatively small in copper but much larger in the stainless steel. Thus in the copper tests (and in the copper-aluminum tests) the temperature rise in the experiments reported here is not significant, whereas that in the stainless steel experiments can not be neglected. This will become evident in the stress strain curves presented below.

Some stress strain curves for the experiments with copper and Nitronic 40 stainless steel are shown in Figs. 3 and 4. Note in Fig. 4 that the curves at strain rates less than 10^{-2} s^{-1} intercept those at higher strain rates. This is a direct consequence of heat generation and the increasing temperature for the higher strain rate experiments. In contrast the results for copper do not show this trend.

The stress strain curves for both copper and Nitronic 40 indicate that the strain rate sensitivity is increasing at high strain rates. It is easier to visualize this increase in a semi-logarithmic plot of flow stress at constant strain versus strain rate. Another advantage of this plot is that by including several sets of data such a plot allows a separation of

effects due to experimental scatter from those due to real changes in flow stress. Semi-logarithmic plots at various strains are shown in Figs. 5 through 8 for all materials tested. In each case an increase in rate sensitivity defined by Eq. 1 is found at strain rates of the SHPB experiments. The stainless steel results in Figs. 7 and 8 suggest that the increased rate sensitivity begins at strain rates as low as 10^2 s^{-1}. It should be noted that none of the experimental errors described in the previous section are important at strain rates as "low" as 10^2 s^{-1}. Thus, this provides further evidence that the increased rate sensitivity found in these materials is real rather than an experimental artifact. In the next section the origin of this increased rate sensitivity will be examined in more detail.

IV. ORIGIN OF THE INCREASED RATE SENSITIVITY AT HIGH STRAIN RATES

Any of the SHPB data shown in Figs. 5 - 8 may be plotted on linear axes and fit to an equation of the form given by Eq. 2. An example for the copper data is shown in Fig. 9. The agreement with Eq. 2 has led some investigators to conclude that the increased rate sensitivity found in this regime is due to a transition to drag controlled deformation, as was described in Section 1 [7,14]. However, the experimentally found value of σ_b has been inconsistent with the theoretical understanding of dislocation/obstacle interactions, which dictates a small, rather than a large value of σ_b [29,30]. To further understand the implications of the results shown in Figs. 5 - 8, it is worthwhile to review some features of dislocation/obstacle interactions.

A schematic of a dislocation restricted by several barriers, separated by an average distance λ is shown in Fig. 10. At equilibrium and at 0 K the force required to proceed past the obstacle array is $\hat{K}$ and the stress $\hat{\tau}$ is written

$$\hat{\tau} = \frac{\hat{K}}{b\lambda} . \qquad (12)$$

This stress is called the threshold stress or the mechanical threshold and is a measure of the intrinsic strength determined by the particular obstacle configuration. Once the dislocation breaks away from the first set of obstacles it will proceed to the next set where the same equilibrium

condition applies. For dislocation/dislocation interactions and for a statistical distribution of dislocations the mechanical threshold stress becomes [31]

$$\hat{\tau} = \alpha \mu b \rho^{1/2} \tag{13}$$

where ρ is the total dislocation density and α is a constant of order 0.5. At temperatures greater than 0 K thermal activation assists the applied stress and thus a lower applied stress is required to force the dislocation past the obstacle. The value of the applied stress now becomes temperature and strain rate dependent; the actual dependencies are given by an Arrhenius expression of the form

$$\dot{\varepsilon} = \dot{\varepsilon}_o \exp - \frac{\Delta G}{kT} , \tag{14}$$

where $\dot{\varepsilon}_o$ is a constant and, for interactions with short range obstacles, the activation energy ΔG is written [31]

$$\Delta G = \mu(T) b^3 g_o \left\{1 - \left(\frac{\sigma}{\hat{\sigma}}\right)^{1/2}\right\}^{3/2} , \tag{15}$$

where g_o is the normalized activation energy and $\hat{\sigma} = M\hat{\tau}$ where M is the Taylor factor (M = 3.06).

These equations do not give a dramatically increasing strain rate sensitivity at high strain rates, which would appear to imply that the increased rate sensitivity found at SHPB strain rates requires a new deformation mechanism. However, the restriction to Eqs. 14 and 15 above is that they describe the temperature and strain rate dependencies of some unique obstacle configuration or "structure", the measure of which is the mechanical threshold. The comparison of experimental results at constant strain in Figs. 5 - 9 may not satisfy this constant structure restriction. Strain rate jump tests have been used to probe the constant structure strain rate sensitivity at lower strain rates. In the SHPB, however, the errors inherent to the measurement of the dynamic yield stress limit these techniques to those materials that exhibit a large constant structure strain rate sensitivity.

Since the constant structure strain rate sensitivity can not be measured directly at high strain rates, the validity of using a plot at

constant strain to approximate one at constant structure can be investigated by measuring the mechanical threshold stress.

A. MEASUREMENT OF THE MECHANICAL THRESHOLD

The procedure for measuring the mechanical threshold stress has been described previously [19,32]. Multiple specimens are deformed at the strain rate of interest to the strain of interest. Then each specimen is reloaded quasi-statically at temperatures of 76 K, ~180 K and 295 K and an extrapolation is made to determine the reload yield stress at 0 K. Combining and rearranging Eqs. 14 and 15 yields

$$\left(\frac{\sigma}{\mu(T)}\right)^{1/2} = \left(\frac{\hat{\sigma}}{\mu(T)}\right)^{1/2} \left[1 - \left(\ln\frac{\dot{\varepsilon}_o}{\dot{\varepsilon}} \frac{kT}{\mu(T)b^3 g_o}\right)^{2/3}\right] . \qquad (16)$$

which indicates that a plot of the square root of the reload yield stress, normalized by the temperature dependent shear modulus, versus test temperature, which is also normalized by the shear modulus and raised to a power of 2/3, should give a straight line. The intercept at 0 K gives the mechanical threshold while the slope of this line is inversely proportional to the normalized activation energy g_o.

A large test matrix was chosen to investigate $\hat{\sigma}$ (ε, $\dot{\varepsilon}$) in copper. Strain rates of 10^{-4}, 10^{-2}, 1, 100, 2000, 5000 and 9500 s^{-1} were chosen and specimens were loaded to strains of 0.05, 0.10, 0.15, 0.20 and 0.25 at each of these strain rates. Thus 35 separate stress and strain rate histories were investigated. In addition, one shock wave recovery experiment was performed at a shock pressure of 10 GPa [33]. A less extensive series of mechanical threshold stress measurements was performed in Nitronic 40. Samples were deformed to a strain of 0.10 at strain rates of 10^{-3} and $6x10^{3}$ s^{-1}.

The results of these studies have been described in [32]. Figure 11 shows the normalized plot suggested by Eq. 16 for copper deformed at a strain rate of 0.000145 s^{-1} to various strains. The intercept at T = 0 K is seen to increase with increasing strain, which is consistent with the behavior expected from Eq. 13. The dislocation density computed from the measured mechanical threshold stresses and Eq. 13 are shown in Fig. 12. A straight line of the form

$$\rho = \rho_o + M\varepsilon \quad , \tag{17}$$

where $M = 11 \times 10^{14}$ m^{-2} and $\rho_o = 0$ can be fit through the results in Fig. 12. Gilman [34] has proposed on theoretical grounds an equation identical to Eq. 17 where M is termed the dislocation multiplication constant. Although Gilman has emphasized that the coefficient M is a measureable parameter that may vary with temperature [34] (and, thus, with strain rate), the coefficient M is generally perceived as a constant. For copper, M is found experimentally to lie within the range of $M = 5 \times 10^{14}$ to 15×10^{14} m^{-2} [15] over a wide range of strain rates, which agrees with the value found in Fig. 12.

The dependence of the threshold stress for copper deformed at various strain rates to a strain of 0.10 is shown in Fig. 13. If constant strain were to imply constant structure, then the mechanical threshold stress, or the intercept at T = 0 K in Fig. 18 should be independent of strain rate. As shown, however, there is a definite strain rate dependence to the mechanical threshold. The data at strains of 0.10 and 0.20 are plotted on the semi-logarithmic axes in Fig. 14. Included in this figure are the flow stress values plotted in Fig. 5. The results in this figure clearly show that the increase in the mechanical threshold stress parallels that of the flow stress. Of particular interest is the behavior at strain rates greater than 10^3 s^{-1} where the increasing rate sensitivity of the flow stress is accompanied by that of the mechanical threshold stress; this is easier to visualize in the linear axes of Fig. 15. By interpolating between the test results at different strain and strain rates, it is possible to generate the plot of flow stress at constant mechanical threshold stress versus strain rate shown in Fig. 16. This plot shows no dramatic increase in rate sensitivity at strain rates exceeding 10^3 s^{-1}, which should be contrasted with the behavior at constant strain shown in Fig. 5.

Measurements in the copper sample shock deformed at 10 GPa [33] gave an even higher value of the mechanical threshold stress than was measured at equivalent strains at strain rates to 10^4 s^{-1}. The history during shock deformation and release is very complicated and, in fact, the strain rates may differ by orders of magnitude between the loading and release processes. The shock process does, however, yield a well defined equivalent plastic strain [35], which in copper shock deformed at 10 GPa is

0.0825. Figure 17 shows the comparison of the mechanical threshold stress at this strain as a function of strain rate. The strain rate for the shock deformation is assumed to lie within the range 10^5 s^{-1} to 10^7 s^{-1}. It is evident from this figure that the increased rate sensitivity of the threshold stress noted at strain rates exceeding ~10^3 s^{-1} continues into the shock regime. Unfortunately, we do not know the value of the flow stress which accompanies the measured mechanical threshold stress for the shock deformed sample. Without the flow stress it is not possible to evaluate the contribution of dislocation drag controlled deformation during the shock deformation.

The results for Nitronic 40 shown in Fig. 18 also indicate an increasing mechanical threshold stress with strain rate, but the increase is much less than the increase in flow stress. This implies that whereas most of the increase in flow stress with strain rate in copper is due to the rate sensitivity of structure evolution, that in Nitronic 40 is primarily due to intrinsic rate sensitivity described by Eq. 13. Thus, an abrupt change in strain rate from a quasi-static to a dynamic strain rate should yield a very small increase in flow stress in copper but a very large increased flow stress in the stainless steel. The results shown in Fig. 19 for a Nitronic 40 sample deformed at a strain rate of 10^{-3} s^{-1} to a strain of 0.10, unloaded, then reloaded at a strain rate of $3x10^3$ s^{-1} tend to verify that most of the rate sensitivity in this material is intrinsic. The increased rate sensitivity at strain rates exceeding ~10^2 s^{-1} in this material is likely related to the increase in the mechanical threshold stress with strain rate, as was found for copper. This, however, needs to be verified with additional measurements of the mechanical threshold stress at intermediate strain rates.

To summarize, these measurements of the mechanical threshold stress have shown that for copper and Nitronic 40 deformed at strain rates less than 10^4 s^{-1}, the flow stress is less than the threshold stress, which indicates that dislocation drag is not responsible for the increased dynamic strain rate sensitivity found in these materials. In copper, the predominant rate sensitivity seen in a plot of stress at constant strain versus strain rate is due to the rate sensitivity of structure evolution. In Nitronic 40 this latter rate sensitivity combines with the intrinsic rate sensitivity to yield the behavior shown in Fig. 18.

One of the conclusions based on the mechanical threshold measurements

and analysis presented here is that Eq. 17, as it is written, is not a valid description of dislocation generation over a wide range of strain rates. This relation treats plastic strain as a structure, or thermodynamic state variable, which we have shown is not appropriate for both copper and Nitronic 40. Clearly the constant M in Eq. 17 must be a function of strain rate, or perhaps stress, as was originally postulated [34]. Previous investigators have measured the dislocation densities in quasi-statically and dynamically deformed copper [15] and aluminum [12,36] using transmission electron microscopy. A large increase in ρ with increasing strain rate was measured in Al single crystals [12] and polycrystals [36], whereas only a small increase was measured in Cu single crystals [15]. It should be noted, however, that TEM techniques to determine dislocation densities in heavily ($\varepsilon > 0.01$) deformed metals are subject to large errors. The ratio of the maximum (for the 10 GPa shock) to the minimum (at $\dot{\varepsilon} = 10^{-4}$ s^{-1}) mechanical threshold stress in Fig. 17 is only 1.8 which, from Eq. 13, implies that the ratio of dislocation densities for these two histories is only ~ 3.2. This may be outside the precision of techniques based on dislocation counting in the TEM when dislocation densities are so high ($\rho \approx 10^{14}$ m^{-2}). For this reason, evidence for the general validity of Eq. 17 based on TEM observations should be regarded with some suspicion. Equation 18 is an approximate but limited rule that should be used only to give a rough estimate of dislocation generation rates in FCC metals.

V. IMPLICATIONS FOR CONSTITUTIVE LAWS

The mechanical threshold measurements in copper and Nitronic 40 lead to several conclusions concerning the choice of numerical models or constitutive laws to describe the mechanical behavior of these materials over a wide range of strain rates. One conclusion concerning the validity of Eq. 17 was discussed in the previous section. For models based on dislocation theory and micromechanisms, it is clear that Eq. 17 is unsuitable for the description of dislocation generation. The main shortcoming of Eq. 17 is that, as written, it implicitly assumes that dislocation densities are equivalent at equivalent strain, i.e., the rate dependence of dislocation generation is ignored.

The above considerations are related to the more general conclusion

that strain is an inappropriate variable to incorporate into a constitutive law as a path independent parameter. This is not a new conclusion, but the danger of assuming that constant strain implies constant structure has been demonstrated here for the interpretation of the increased rate sensitivity found at strain rates exceeding ~10^3 s^{-1}. These results reemphasize the importance of incorporating some form of an internal state variable into constitutive laws. This is an essential feature of recent numerical procedures proposed by Bammann [37] and others.

Another conclusion based on the results reported here is that the constant structure (or intrinsic) strain rate sensitivity does not increase dramatically in the FCC metals considered as the strain rate is raised above ~10^3 s^{-1}. Although the actual stress-strain rate behavior may be describable by an equation of the form of Eq. 1, this equation overestimates the actual rate sensitivity. Thus when this equation is incorporated into a numerical model that is used to describe deformation in a component in which the strain rate is changing, the predicted behavior may differ greatly from the actual behavior of the material. This may be important, for instance, in the prediction of the formation of instabilities in plastic flow [58]. Use of a constitutive law in the form of Eq. 2 can overestimate the stabilizing influence of strain rate in such problems. Our results suggest that the strain rate dependence of the flow stress in copper, copper-aluminum alloys, and austenitic stainless steels should remain in the format given by Eqs. 14 and 15 or, equivalently, in the form

$$\frac{\sigma}{\sigma_o} = \left(\frac{\dot{\varepsilon}}{\dot{\varepsilon}_o}\right)^m , \tag{18}$$

where $m \ll 1$. Indeed, recent formulations proposed by Johnson [39] and Bammann [37] retain the low intrinsic rate dependence given by these expressions.

VI. SUMMARY

This paper has included two major themes. The first considered the validity of experimental results determined with SHPB techniques. It was concluded that these techniques can yield valid dynamic stress strain data provided that certain precautions regarding lubrication, specimen aspect

ratio, and limiting strain rates are practiced. There are additional features of the data reported in Section III that support the validity of the results; these are listed below.

1) Although not emphasized previously, the SHPB results reported in Figs. 5 - 9 were obtained with two and, for the copper results in Figs. 5 and 9, three different bar sizes [19]. Decreasing the diameter of the pressure bar, and thus the diameter (but not the aspect ratio) of the specimen allows, from Eq. 4 and the discussion in [27], higher strain rates. The fact that similar results were obtained with different bar diameters provides confidence in test results.

2) The main question regarding dynamic test results in the SHPB is whether or not there exists an increasing strain rate sensitivity at high strain rates. The results for the austenitic stainless steels shown in Figs 7 and 8 show a clear trend with strain rate, with an increasing rate sensitivity beginning at strain rates well below the region where inertia considerations are important; this is further evidence in support of the validity of the test results.

3) Finally, we note that the mechanical threshold values also showed an increasing dynamic rate sensitivity. This is strong evidence that the corresponding increased rate sensitivity of the flow stress values represents actual material behavior since the ratio $\sigma/\hat{\sigma}$ can not decrease with increasing strain rate.

The major theme of this paper then was to evaluate the source of this increased strain rate sensitivity. Measurements of the mechanical threshold stress coupled with an analysis of the kinetics of dislocation-obstacle interactions led to the conclusion that the increased rate sensitivity found in a plot of flow stress at constant strain versus strain rate arises from the rate sensitivity of structure evolution rather than from any change in deformation mechanism. In the copper, copper-alluminum alloys and austentic stainless steels evaluated at strain rates less than $\sim 10^4$ s^{-1}, dislocation drag mechanisms are not rate controlling.

This result implies that viscous laws such as Eq. 2 should not be incorporated into constitutive descriptions of material behavior under these conditions since the low strain rate sensitivity of thermal activation controlled deformation is maintained to strain rates as high as 10^4 s^{-1} in these materials. However, any description of constitutive

behavior over a wide range of strain rates needs to account for the rate dependence of structure evolution. Although this can be done empirically by measuring $\hat{\sigma}(\dot{\varepsilon},\varepsilon)$, as was reported here, theoretical descriptions of dislocation generation processes might be very useful in eventually leading to complete descriptions of constitutive behavior in FCC metals and alloys as well as in metals of other crystal structures.

ACKNOWLEDGEMENTS

I would like to acknowledge the many contributions made to the experimental program by C. E. Frantz and the assistance of W. J. Wright and M. Lopez on the measurements reported in this report. I am also grateful for the extensive collaborations with U. F. Kocks and G. Regazzoni. This work was performed under the auspices of the U. S. Department of Energy.

REFERENCES

1. A. J. Holzer, J. Engr. Mat. Tech. 101:231 (1979).

2. F. E. Hauser, J. A. Simmons and J. E. Dorn, "Strain Rate Effects in Plastic Wave Propagation," in Response of Metals to High Velocity Deformation, P. G. Shewmon and V. F. Zackay (eds.), Interscience, New York, 1961.

3. U. S. Lindholm, J. Mech. Phys. Solids 12:317 (1964).

4. C. H. Karnes and E. A. Ripperger, J. Mech. Phys. Solids 14:75 (1966).

5. D. L. Holt, S. G. Babcock, S. J. Green and C. J. Maiden, "The Strain Rate Dependence of the Flow Stress in some Aluminum Alloys," General Motors Research Laboratories TR66-75, 1966.

6. W. G. Ferguson, A. Kumar and J. E. Dorn, J. Appl. Phys. 30:1863 (1967).

7. A. Kumar, F. E. Hauser and J. E. Dorn, Acta Meta. 16:1189 (1968).

8. U. S. Lindholm and L. M. Yeakley, Exp. Mech. 8:1 (1968).

9. C. K. H. Dharan and F. E. Hauser, Exp. Mech. 10:370 (1970).

10. S. J. Green, C. J. Maiden, S. G. Babcock and F. L. Schierloh, "The High Strain-Rate Behavior of Face-Centered Cubic Metals," in Inelastic Behavior of Solids, M. Kanninen, W. Adler, A. Rosenfield and R. Jaffee (eds.), McGraw-Hill Co., New York, 1970.

11. U. S. Lindholm, "Deformation Maps in the Region of High Dislocation Velocity," in High Velocity Deformation of Solids, K. Kawata and J. Shiojri (eds.), Springer-Verlag, New York, 1978.

12. C. Y. Chiem and J. Duffy, "Strain Rate History Effects and Observations of Dislocation Substructure in Aluminum Single Crystals Following Dynamic Deformation," Materials Research Laboratory, Brown University, MRL E-137, 1981.

13. E. A. Ripperger, "Dynamic Plastic Behavior of Aluminum, Copper and Iron," in Behavior of Materials Under Dynamic Loading, N. J. Huffington (ed.), Am. Soc. Mech. Engr., Chicago, 1965.

14. A. Kumar and R. G. Kumble, J. Appl. Phys. 40:3475 (1969).

15. J. W. Edington, Phil. Mag. 19:1189 (1969).

16. F. Dusek, Z. Jasinski, J. Buchar, A. Litwora and A. Piatkowski, Czech. J. Phys. B26:538 (1976).

17. M. Stelly and R. Dormeval, "Some Results on the Dynamic Deformation of Copper," in High Velocity Deformation of Solids, K. Kawata and J. Shioiri (eds.), Springer-Verlag, New York, 1978.

18. J. Shioiri, K. Satoh and K. Nishimura, " Experimental Studies on the Behavior of Dislocations in Copper at High Rates of Strain," in High Velocity Deformation of Solids, K. Kawata and J. Shioiri (eds.), Springer-Verlag, New York, 1978.

19. P. S. Follansbee, G. Regazzoni and U. F. Kocks, "The Transition to Drag-Controlled Deformation in Copper at High Strain Rates," in Mechanical Properties at High Rates of Strain, J. Harding (ed.), Institute of Physics, London, 1984.

20. M. Malatynski and J. Klepaczko, Int. J. Mech. Sci. 22:173 (1980).

21. T. Muller, J. Mech. Engr. Sci. 14:3 (1972).

22. A. V. Granato, "Microscopic Mechanisms of Dislocation Drag," in Metallurgical Effects at High Strain Rates, R. W. Rohde, B. M. Butcher, J. R. Holland and C.H. Karnes (eds.), Plenum Press, New York, 1973.

23. U. S. Lindholm, in Techniques of Metals Research, Vol. 5, part 1, R. F. Bunshah (ed.), John Wiley and Sons, New York, 1971, Chap. 4, p. 199.

24. P. S. Follansbee, in Metals Handbook, Ninth Edition, Vol. 8, Am. Soc. Metals, Metals Park, Ohio, 1985, p. 198.

25. E. D. H. Davies and S. C. Hunter, J. Mech. Phys. Solids 11:155 (1963).

26. L. D. Bertholf and C. H. Karnes, J. Mech. Phys. Solids 23:1 (1975).

27. C. E. Frantz, P. S. Follansbee and W. J. Wright, "Experimental Techniques with the Split Hopkinson Pressure Bar," in High Energy Rate Fabrication, I. Berman and J. W. Schroeder (eds.), Am. Soc. Mech. Engr., New York, 1984.

28. P. S. Follansbee and C. E. Frantz, J. Engr. Mat. Tech. 105:61 (1983).

29. D. Klahn, A. K. Mukherjee and J. E. Dorn, "Strain-Rate Effects," in Sec. Int. Conf. on the Strength of Metals and Alloys, Am. Soc. Metals, 1970.

30. H. J. Frost and M. F. Ashby, J. Appl. Phys. 42:5273 (1971).

31. U. F. Kocks, A. S. Argon and M. F. Ashby, Thermodynamics and Kinetics of Slip, Prog. Mtl. Sci. 19, Pergamon Press, New York, 1975.

32. P. S. Follansbee, U. F. Kocks and G. Regazzoni, "The Mechanical Threshold of Dynamically Deformed Copper and Nitronic 40," to be published in Proc. Int. Conf. on Mechanical and Physical Behavior of Materials under Dynamic Loading, Paris, France, 1985.

33. P. S. Follansbee and G. T. Gray, "Threshold Stress Measurements in Shock-Deformed Copper," to be published in Proc. Am. Phys. Soc. Topical Conf. on Shock Waves in Condensed Matter, Spokane, Washington, 1985.

34. J. J. Gilman, Appl. Mech. Rev. 21:767 (1968).

35. A. H. Holtzman and G. R. Cowan, "The Strengthening of Austenitic Manganese Steel by Plane Shock Waves," in Response of Metals t· High Velocity Deformation, P. G. Shewmon and V. F. Zackay (eds.), Interscience, New York, 1961.

36. A. Korbel and K. Swiatkowski, Met. Sci. J. 6:60 (1972).

37. D. J. Bammann, "An Internal Variable Model of Elastic-Viscoplasticity," in Mechanics of Dislocations, E. C. Aifantis and J. P. Hirth (eds.), Am. Soc. Metals, Metals Park, Ohio, 1985.

38. G. Regazzoni, J. N. Johnson and P. S. Follansbee, "Theoretical Study of the Dynamic Tensile Test," submitted to J. Appl. Mech. (1985).

39. G. R. Johnson, J. Engr. Mat. Tech. 103:201 (1981).

Table 1. Previous Investigations of High Rate Deformation of FCC Metals

Reference	Maximum $\dot{\varepsilon}$ (10^3 s^{-1})	Material	Rate Sensitivity
Hauser et al [2]	15	pxtl Al	I(ncreasing)
Lindholm [3]	2	pxtl Al,Cu,Pb	C(onstant)
Karnes and Ripperger [4]	4	pxtl Al	I
Holt et al [5]	1	Al alloys:	
		7075, 6061	C
Ferguson et al [6]	10	sxtl Al	I
Kumar et al [7]	26	sxtl Al	I
Lindholm and Yeakley [8]	2.6	1100 Al	I
Dharan and Hauser [9]	120	pxtl Al	I
Green et al [10]	1	1060 Al, Pb	
		OFHC Cu,Ni	C
Lindholm [11]	60	1100 Al	I
		pxtl Cu	C
Chiem and Duffy [12]	5	sxtl Al	I
Ripperger [13]	5	OFHC Cu	I
Kumar and Kumble [14]	2	pxtl Cu	I
Edington [15]	10	sxtl Cu	I
Dusek et al [16]	10	sxtl Cu	I
Stelly and Dormeval [17]	20	sxtl Cu	I
Shioiri et al [18]	2.5	OFHC Cu	I
Follansbee et al [19]	30	OFE Cu	I
Malatynski and Klepaczko [20]	2	pxtl Pb	I
Muller [21]	10	pxtl Ni	I

Table 2 Compositions* of Stainless Steels Tested

Element	AISI 304	AISI 304L	AISI 310S	AISI 316L	Nitronic 40
Cr	18.25	18.27	24.72	17.10	20.01
Ni	8.35	8.81	19.39	10.95	7.10
Mn	1.29	1.40	1.64	1.49	8.92
Mo	0.23	0.31	0.10	2.13	0.14
Si	0.29	0.33	0.54	0.61	0.70
Cu	0.47	0.43	0.08	0.54	0.40
C	0.05	0.015	0.067	0.012	0.02
P	0.037	0.027	0.018	0.025	0.023
S	0.024	0.018	0.008	0.005	0.002
N	0.09	0.083	---	0.099	0.32

* In weight percent.

Table 3 Thermal properties and estimated temperature rise and flow stress decrease for adiabatic deformation * of copper and Nitronic 40

	$\rho C_p \left(\frac{MPa}{K}\right)$	$\int \sigma(\varepsilon) d\varepsilon$ (MPa)	ΔT (K)	$\Delta \sigma$ (MPa)
Copper	3.43	41.2	12	1
Nitronic 40	3.60	221.2	62	125

* $\dot{\varepsilon} \approx 5000\ s^{-1}$; $\varepsilon = 0.20$

FIGURE CAPTIONS

FIG. 1 Schematic of the split Hopkinson pressure bar showing the two, long elastic pressure bars separated by the plastically deforming specimen.

FIG. 2 Dynamic ($\dot{\varepsilon}$ = 6000 s^{-1}) stress strain curve for Nitronic 40 illustrating the difference between the 3-wave analysis (solid line) and the 2-wave analysis (dashed line).

FIG. 3 Stress strain curves for copper measured over a wide range of strain rates. The oscillations in the two curves at the highest strain rates are "Pochhammer - Chree" oscillations and arise from dispersion of the elastic waves in the pressure bars [28].

FIG. 4 Stress strain curves for Nitronic 40 stainless steel measured over a wide range of strain rates. The oscillations in the test at ε = 5000 s^{-1} have been removed by smoothing. (See dashed lines in Fig. 3.)

FIG. 5 Flow stress measured at constant strain versus strain rate for copper.

FIG. 6 Flow stress measured at a constant strain of ε = 0.20 versus strain rate for Cu - 0.2 Al, Cu - 2 Al and Cu - 6 Al.

FIG. 7 Flow stress measured at a constant strain of ε = 0.10 versus strain rate for Nitronic 40 and 316L stainless steels.

FIG. 8 Flow stress measured at a constant strain of ε = 0.10 versus strain rate for 304 (left abscissa), 304L (left abscissa) and 310S (right abscissa) stainless steels.

FIG. 9 Flow stress measured at constant strain versus strain rate (on a linear axis) for copper. (Data at $\dot{\varepsilon} < 10^3$ s^{-1} omitted.)

FIG. 10 Schematic illustration showing the interaction of a dislocation with an idealized array of obstacles of strength K (at 0 K).

FIG. 11 Reload yield stress (σ) versus reload test temperature (T) according to the normalized coordinates suggested by Eq. 16 for copper specimens prestrained at a strain rate of 0.00014 s^{-1} to the strains indicated.

FIG. 12 Total dislocation density, determined from the data shown in Fig. 11 and Eq. 13, versus strain for copper specimens deformed at a strain rate of 0.00014 s^{-1}.

FIG. 13 Normalized plot of reload yield stress versus reload test temperature for copper specimens deformed at the strain rates indicated to a strain of ε = 0.10.

FIG. 14 Semi-logarithmic plot showing the measured flow stress and mechanical threshold stress values at strains of 0.10 and 0.20 versus strain rate for copper deformed at a wide range of strain rates.

FIG. 15 Measured flow stress and mechanical threshold stress values for copper plotted versus strain rate on a linear axis.

FIG. 16 Flow stress at the threshold stress values indicated versus strain rate for copper. This plot at constant threshold stress should be contrasted with the behavior at constant strain shown in Fig. 5.

FIG. 17 Mechanical threshold stress at a strain of 0.0825 versus strain rate. Included in this plot is the data a copper specimen shock-deformed at a shock pressure of 10 GPa.

FIG. 18 FLow stress and mechanical threshold stress values for Nitronic 40 deformed to a strain of $\varepsilon = 0.10$.

FIG. 19 Stress strain curves for Nitronic 40 specimens deformed at strain rates of 0.002 s^{-1} and 3000 s^{-1} and for one specimen deformed at the lower strain rate to a strain of 0.10, unloaded, then reloaded at the higher strain rate.

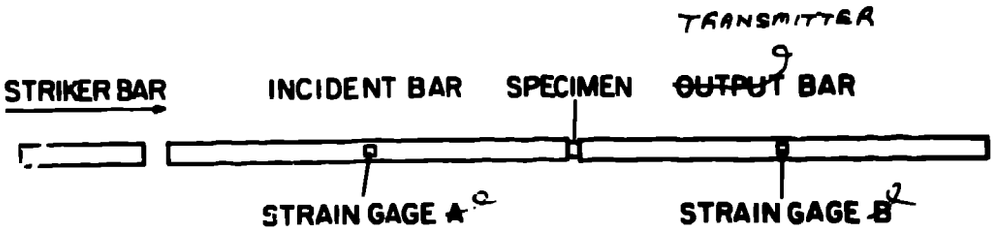

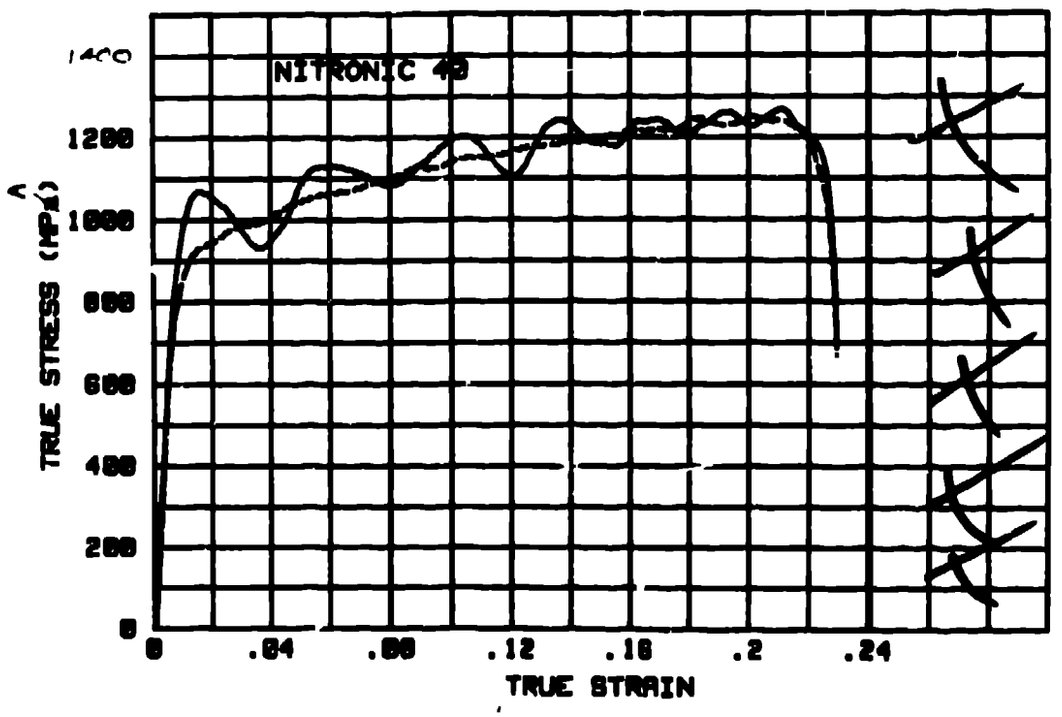

Delete grid lines! ... marks on all axes

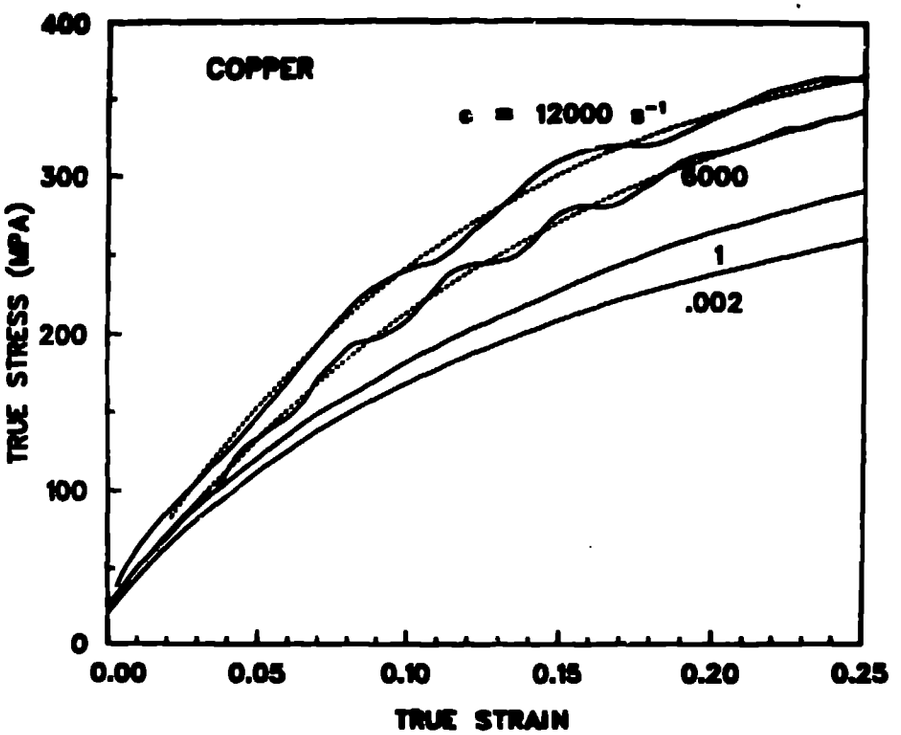
COPPER
ε = 12000 s⁻¹
6000
1
.002
TRUE STRESS (MPA)
400
300
200
100
0
0.00
0.05
0.10
0.15
0.20
0.25
TRUE STRAIN

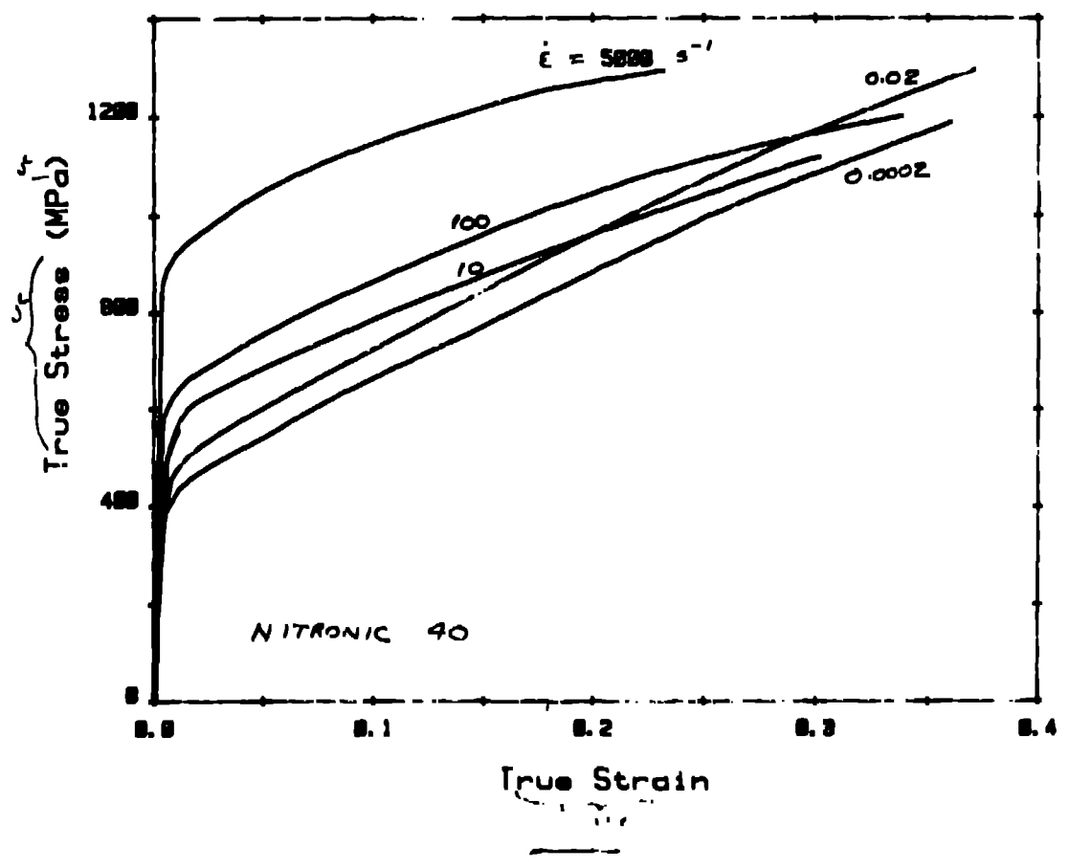
$\dot{\varepsilon}$ = 5000 s⁻¹
0.02
0.0002
100
10
NITRONIC 40
True Stress (MPa)
True Strain

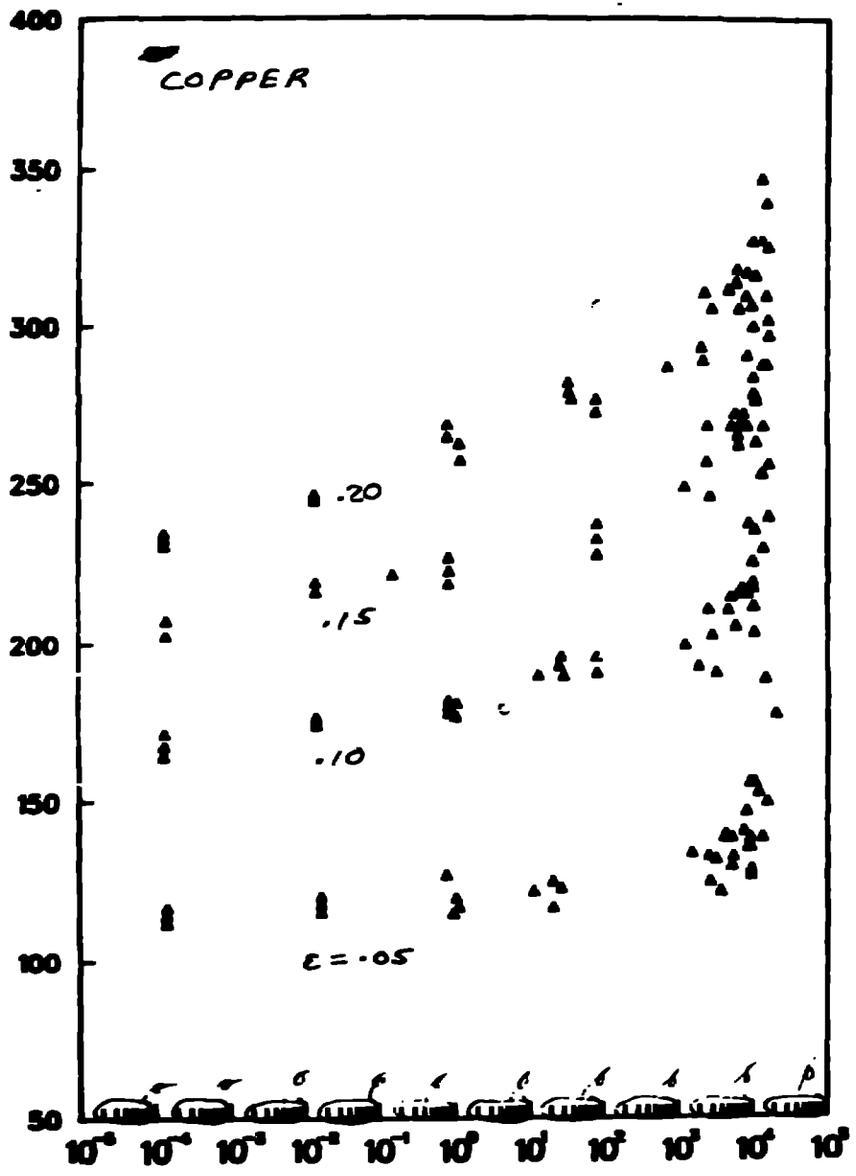
COPPER
400
350
300
250
200
150
100
50
.20
.15
.10
ε = .05
10⁻⁶ 10⁻⁵ 10⁻⁴ 10⁻³ 10⁻² 10⁻¹ 10⁰ 10¹ 10² 10³ 10⁴ 10⁵

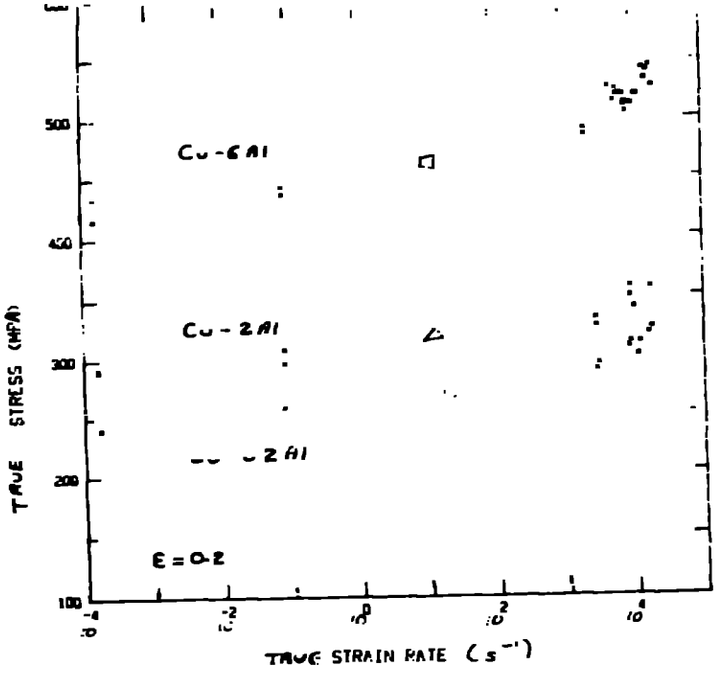
Cu-6Al
Cu-2Al
ε = 0.2
TRUE STRESS (MPa)
TRUE STRAIN RATE (s⁻¹)

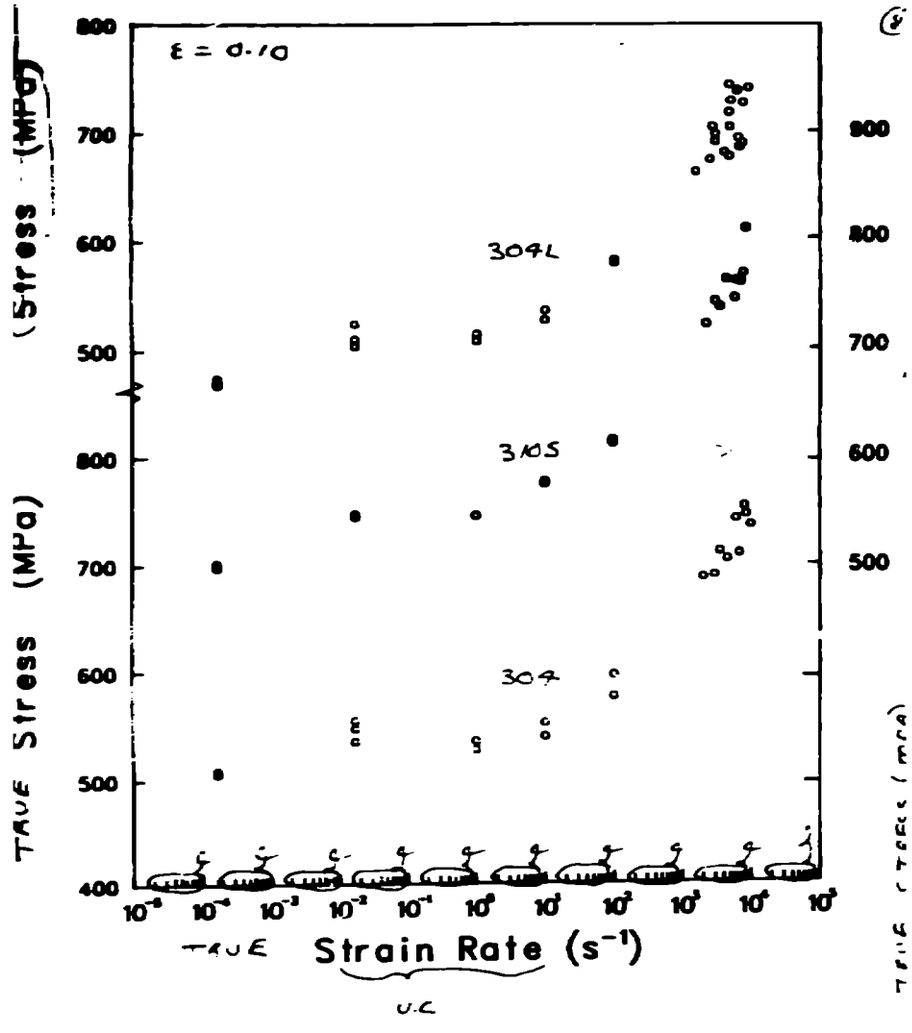
ε = 0.10
304L
316L
304
TRUE Stress (MPa)
TRUE Strain Rate (s⁻¹)

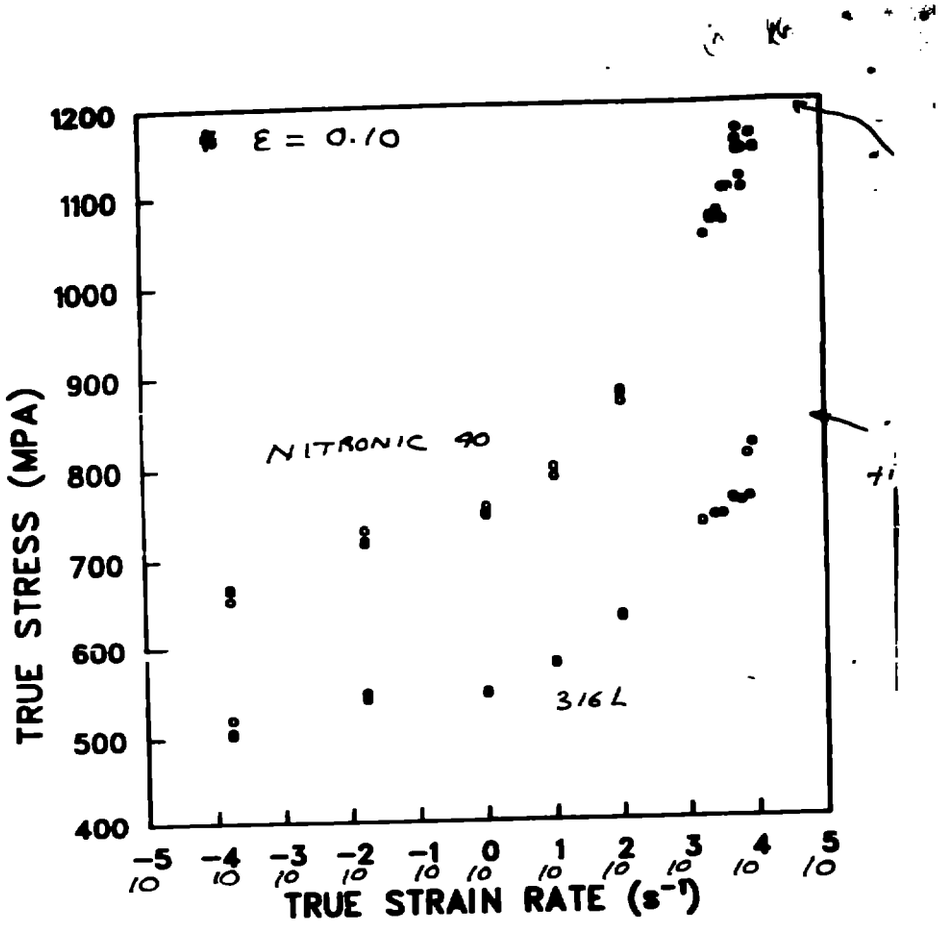
ε = 0.10
NITRONIC 40
316L
TRUE STRESS (MPA)
TRUE STRAIN RATE (s⁻¹)

(9)

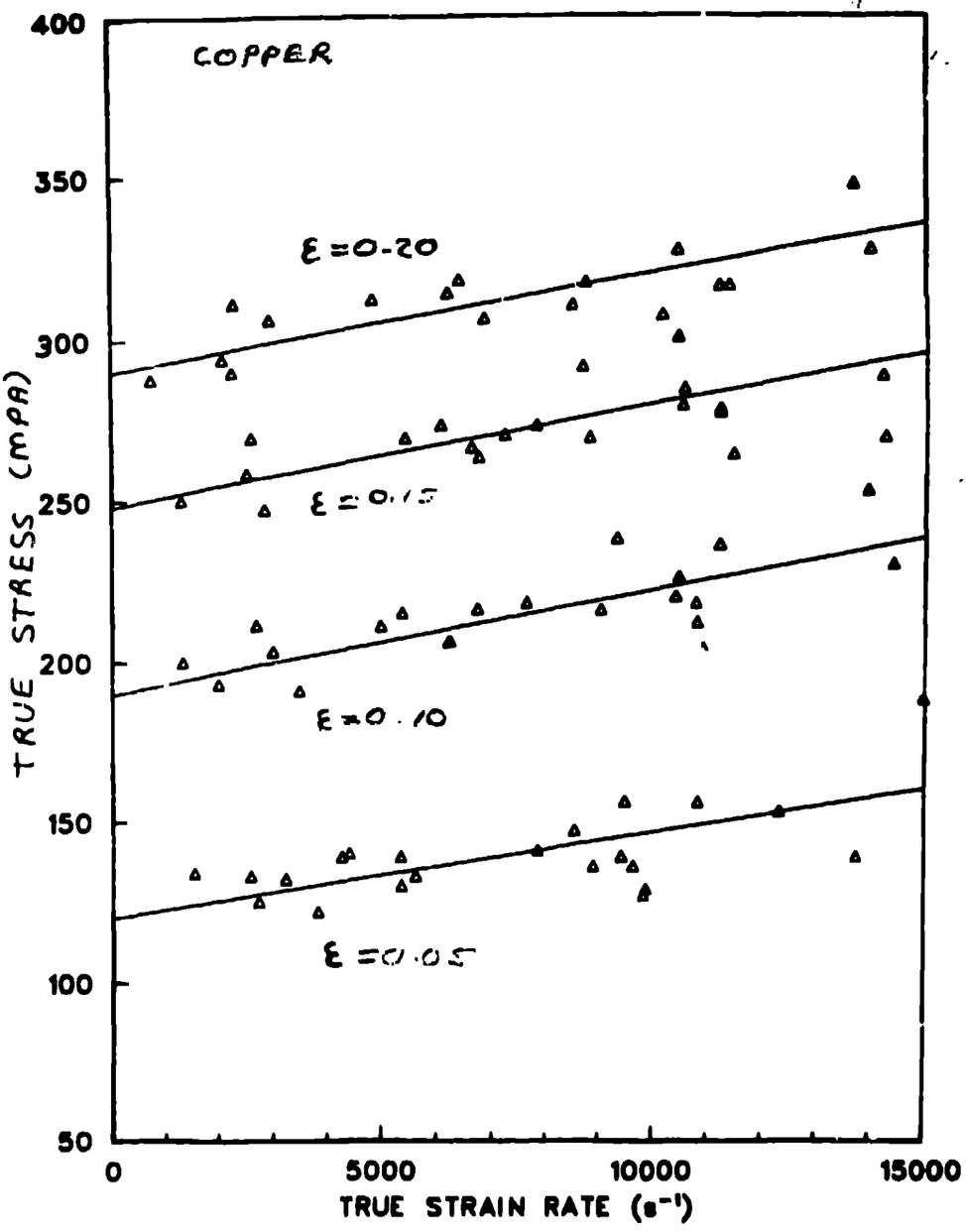
COPPER
ε=0·20
ε=0·15
ε=0·10
ε=0·05
TRUE STRESS (MPA)
TRUE STRAIN RATE (s⁻¹)
400
350
300
250
200
150
100
50
0
5000
10000
15000

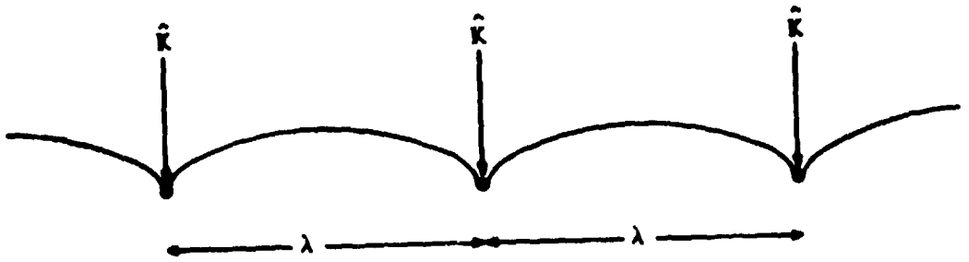
$\hat{K}$
$\hat{K}$
$\hat{K}$
λ
λ

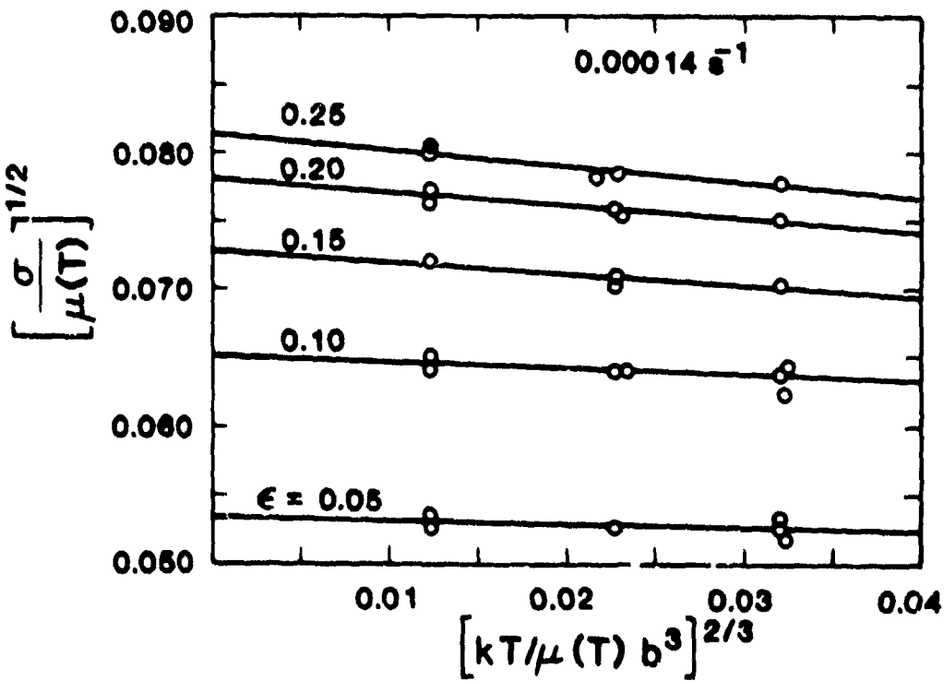
0.090
0.080
0.070
0.060
0.050
0.00014 s⁻¹
0.25
0.20
0.15
0.10
ϵ = 0.05
0.01
0.02
0.03
0.04
$\left[\frac{\sigma}{\mu(T)}\right]^{1/2}$
$\left[kT/\mu(T)\, b^3\right]^{2/3}$

COPPER
$\dot{\varepsilon}$ = 0.00014 s^{-1}
DISLOCATION DENSITY (10^{14} m^{-2})
TRUE STRAIN
0
.05
.10
.15
.20
.25
0.5
1.0
1.5
2.0
2.5
3.0

$\left[\frac{\sigma}{\mu(T)}\right]^{1/2}$
0.060
0.065
0.070
0.075
ε = 0.10
0.00014 s^{-1}
0.82 s^{-1}
6000 s^{-1}
$[1.77/\mu(T)\, b]^{2/3}$
0
0.01
0.02
0.03
0.04

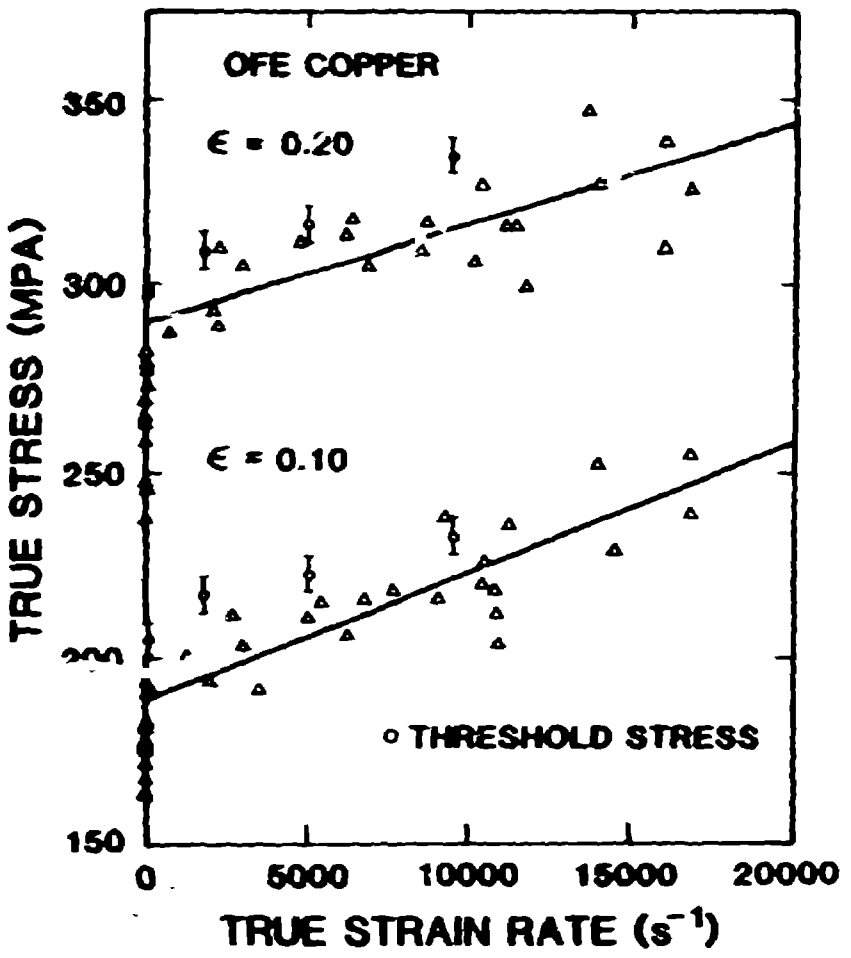
OFE COPPER
ϵ = 0.20
ϵ = 0.10
THRESHOLD STRESS
TRUE STRESS (MPA)
350
300
250
150
0
5000
10000
15000
20000
TRUE STRAIN RATE (s⁻¹)

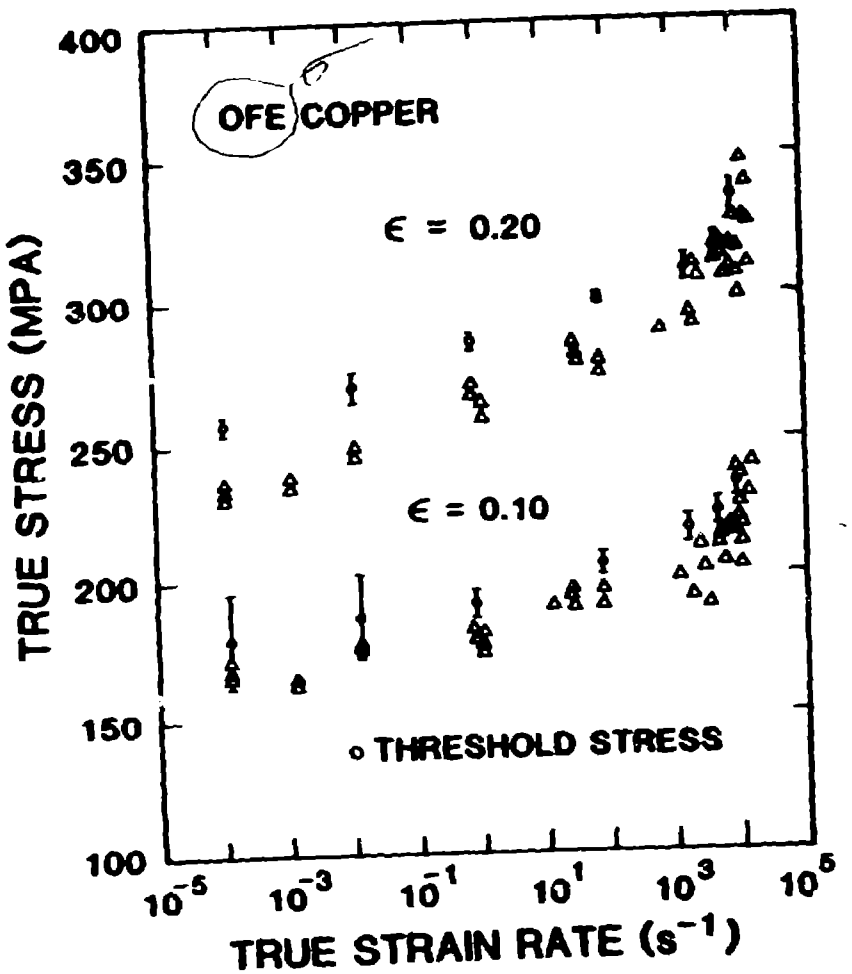
OFE COPPER
ϵ = 0.20
ϵ = 0.10
THRESHOLD STRESS
TRUE STRESS (MPA)
400
350
300
250
200
150
100
10⁻⁵
10⁻³
10⁻¹
10¹
10³
10⁵
TRUE STRAIN RATE (s⁻¹)

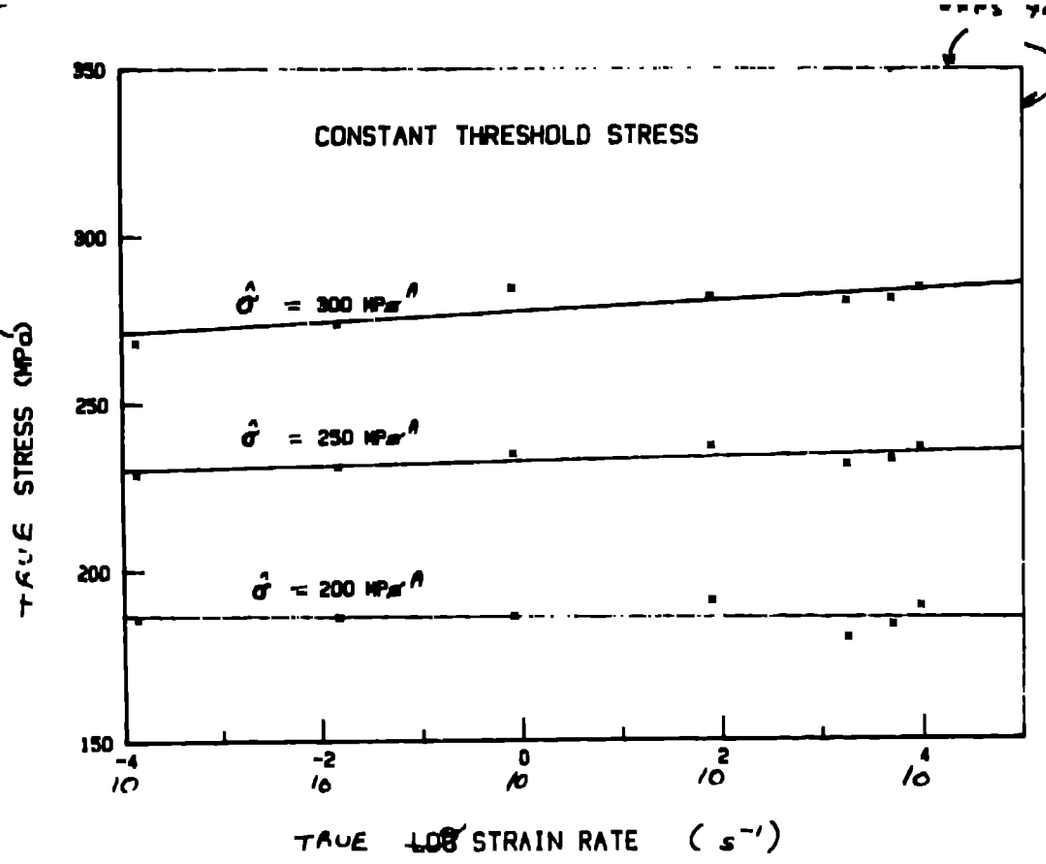
CONSTANT THRESHOLD STRESS
$\hat{\sigma}$ = 300 MPa$\sqrt{m}$
$\hat{\sigma}$ = 250 MPa$\sqrt{m}$
$\hat{\sigma}$ = 200 MPa$\sqrt{m}$
TRUE STRESS (MPa)
350
300
250
200
150
10^{-4}
10^{-2}
10^{0}
10^{2}
10^{4}
TRUE LOG STRAIN RATE (s^{-1})

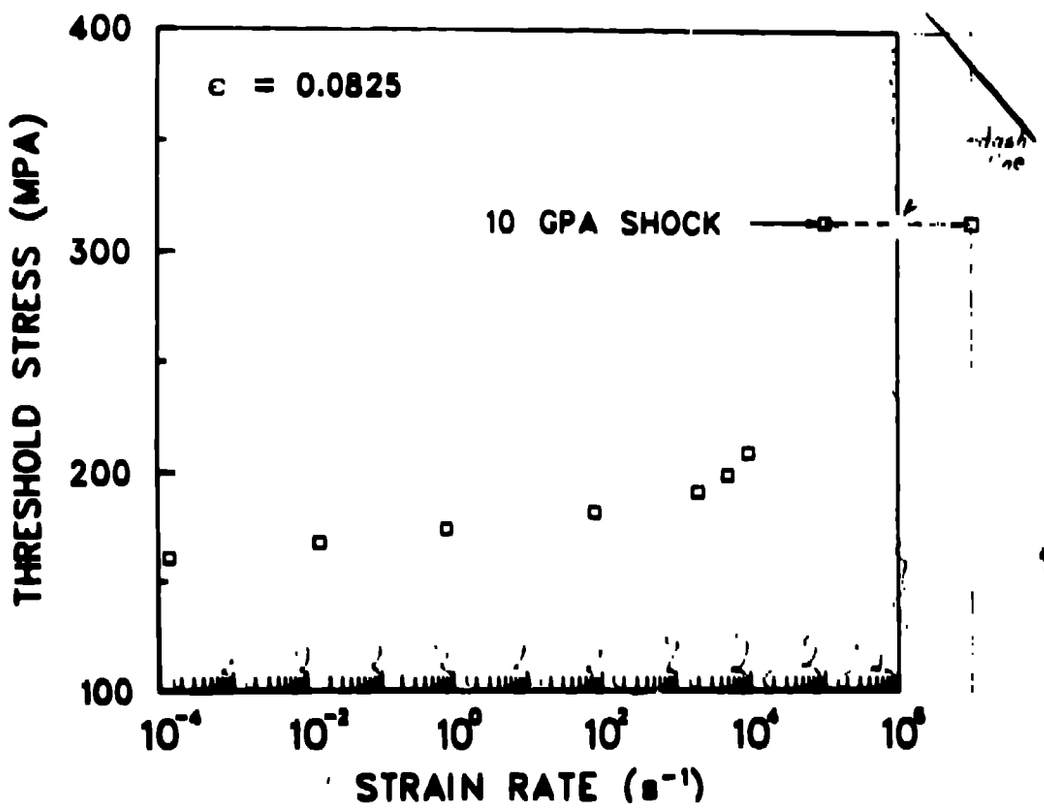
ϵ = 0.0825
10 GPA SHOCK
THRESHOLD STRESS (MPA)
400
300
200
100
10^{-4}
10^{-2}
10^{0}
10^{2}
10^{4}
10^{6}
STRAIN RATE (s^{-1})

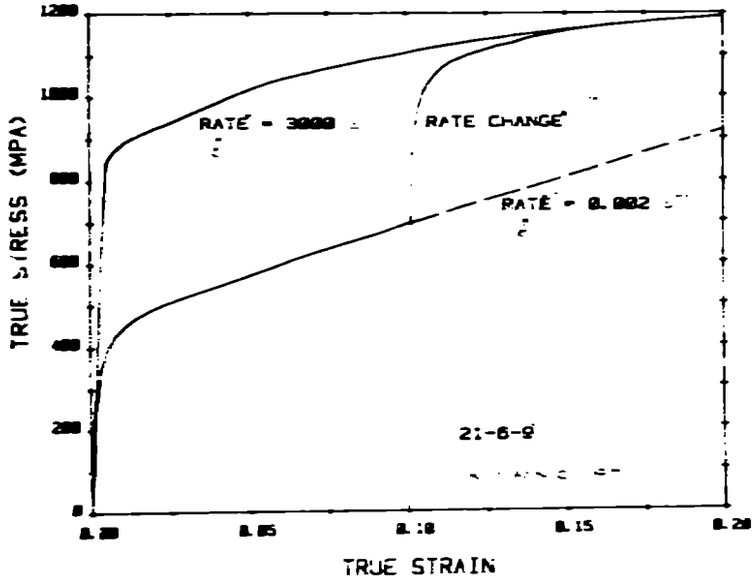
TRUE STRESS (MPA)
RATE CHANGE
21-6-9
TRUE STRAIN

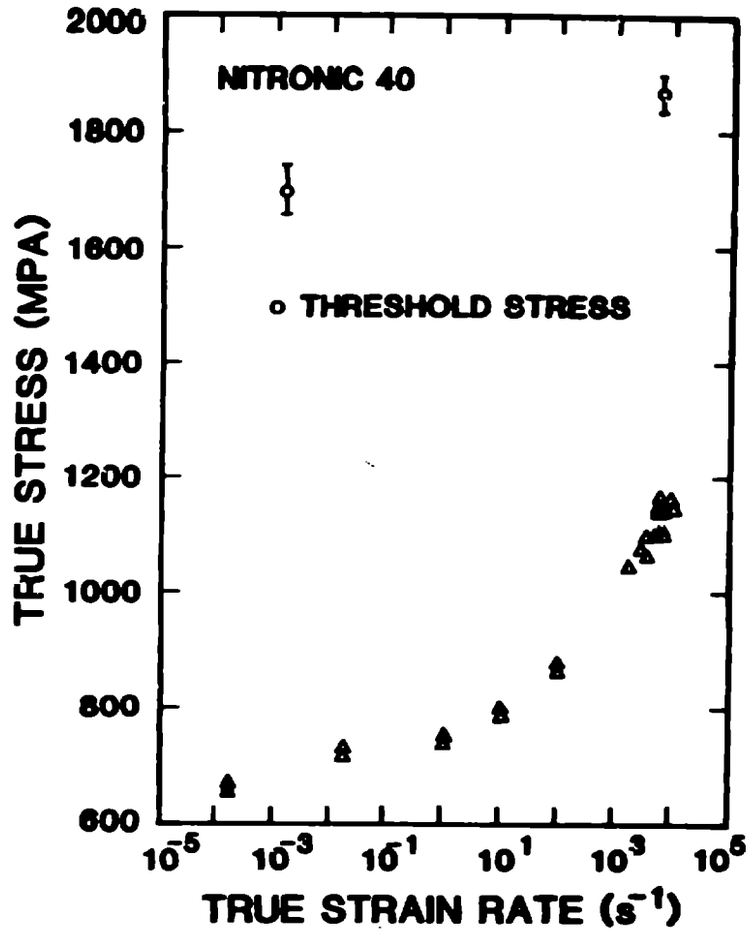
NITRONIC 40
o THRESHOLD STRESS
TRUE STRESS (MPA)
2000
1800
1600
1400
1200
1000
800
600
10^{-5}
10^{-3}
10^{-1}
10^{1}
10^{3}
10^{5}
TRUE STRAIN RATE (s^{-1})